MATERIALS SCIENCE

Large-scale polymeric carbon nanotube membranes with sub–1.27-nm pores

Robert L. McGinnis,[1] Kevin Reimund,[1,2] Jian Ren,[2] Lingling Xia,[2] Maqsud R. Chowdhury,[2] Xuanhao Sun,[2] Maritza Abril,[2] Joshua D. Moon,[3] Melanie M. Merrick,[3] Jaesung Park,[3] Kevin A. Stevens,[3] Jeffrey R. McCutcheon,[2] Benny D. Freeman[3]*

Copyright © 2018 The Authors, some rights reserved; exclusive licensee American Association for the Advancement of Science. No claim to original U.S. Government Works. Distributed under a Creative Commons Attribution NonCommercial License 4.0 (CC BY-NC).

We report the first characterization study of commercial prototype carbon nanotube (CNT) membranes consisting of sub–1.27-nm-diameter CNTs traversing a large-area nonporous polysulfone film. The membranes show rejection of NaCl and $MgSO_4$ at higher ionic strengths than have previously been reported in CNT membranes, and specific size selectivity for analytes with diameters below 1.24 nm. The CNTs used in the membranes were arc discharge nanotubes with inner diameters of 0.67 to 1.27 nm. Water flow through the membranes was 1000 times higher than predicted by Hagen-Poiseuille flow, in agreement with previous CNT membrane studies. Ideal gas selectivity was found to deviate significantly from that predicted by both viscous and Knudsen flow, suggesting that surface diffusion effects may begin to dominate gas selectivity at this size scale.

INTRODUCTION

Membranes for nanofiltration (NF), reverse osmosis (RO), and forward osmosis (FO) are designed for aqueous separation of small molecules (<1000 Da) and dissolved salts. They suffer from limitations in their selectivity, permeability, and chemical resistance, particularly with respect to oxidants, which hampers the effectiveness of fouling mitigation (*1*, *2*). The development of membranes based on novel nanoscale materials, such as carbon nanotubes (CNTs), graphene, and biological or biomimetic pores, has been proposed to address these limitations (*3*–*12*).

Previous studies of CNT membranes have shown that enhanced flow of water and gases through the interior of CNTs can result in very high membrane permeabilities (*3*–*7*). Modeling has predicted that subnanometer CNTs will be capable of high salt rejections in highly saline waters, such as seawater desalination (*6*). Furthermore, the physical and chemical robustness of CNTs may allow aggressive cleaning techniques, such as bleach or other oxidants, which are currently unavailable to conventional membranes for NF, RO, and FO (*13*).

The availability of techniques for precise sorting of CNTs by diameter may enable the fabrication of membranes with a wide range of selectivity. Tight control of CNT fabrication for making batches of CNTs with narrow diameter distribution or monochiral chemistry offers the potential for angstrom-level selectivity of molecules based on size (*14*). For instance, in gas separations, membranes with pores in the subnanometer range have demonstrated gas selectivity, and CNT materials are available in subnanometer diameters, indicating that CNT membranes may be practical for these separations, including separating CO_2 from air or flue gases, O_2 and N_2, alkanes and alkenes, and CO_2 and CH_4, based on both size exclusion and condensability phenomena, depending on the sizes of CNTs and the gases involved (*15*–*17*). The primary limitations in the fabrication of CNT membranes consisting of small CNTs traversing a nonporous polymer film have been the scalability of the fabrication process used, the expected cost of these membranes at commercial scale, and the difficulty of using subnanometer CNTs for membrane fabrication, particularly because these CNTs have not been shown to readily grow in alignment (*18*).

[1]Mattershift, New York, NY 10017, USA. [2]University of Connecticut, Storrs, CT 06269, USA. [3]University of Texas, Austin, TX 78712, USA.
*Corresponding author. Email: freeman@che.utexas.edu

RESULTS

We report here the first experimental study of aligned CNT membranes consisting of CNTs with inner diameters (IDs) smaller than 1.27 nm embedded in a large-scale dense polysulfone polymer matrix, as well as the first study of subnanometer CNT membranes that examine both water and gas transport. The type of CNTs incorporated into membranes in this study was arc discharge (AD) nanotubes with IDs between 0.67 and 1.27 nm (*7*, *19*, *20*). The sample format was a flexible polymer sheet approximately 8″ × 11″ (20.3 cm by 27.9 cm), with a gray coloring (shown in Fig. 1A, inset), a larger scale of fabrication for single-walled CNT membranes than has been reported previously. The methods of fabrication for these membranes have been described by the manufacturer previously in the patent literature (*21*, *22*). The membranes were received from the manufacturer and tested without modification.

Scanning electron microscopy (SEM) and transmission electron microscopy (TEM) images of the CNT membrane, showing the orientation and density of the CNTs, are shown in Fig. 1 (A to C). The images indicate that the average tube density of the CNT membranes is approximately 250 CNTs/μm^2. This density is the same order of magnitude reported for studies of membranes consisting of chemical vapor deposition aligned-growth multiwalled CNT and filter-aligned AD CNT membranes, but approximately $^1/_{10}$ the density reported for aligned-growth double-walled CNT membranes (*3*, *4*, *23*).

A cross-flow RO system was used to test the membranes in aqueous separations (fig. S1). Tests included pure water permeability and the rejection of a series of analytes, including salts and small–molecular weight dyes spanning a range of diameters from 0.72 to 2.3 nm. The dyes were tested with and without the presence of a 2000-ppm (parts per million) NaCl (34 mM) background electrolyte to discriminate between charged-based and size-based steric exclusion effects.

The pure water permeability of the membranes was 5.1 ± 0.4 liter m^{-2} h^{-1} bar^{-1} (LMH)/bar. This membrane permeability represents an enhancement over Hagen-Poiseuille flow of approximately 1000, in the same range as those in previous findings of enhanced water flow through CNT membranes (*3*, *4*). The rejections of the analytes, along with their dimensions, are shown in Fig. 2. The high rejection of chlorophyllin indicates that any defects in the membrane, if present, may be estimated to be below 1.24 nm in size, the narrowest

Downloaded from http://advances.sciencemag.org/ on November 17, 2019

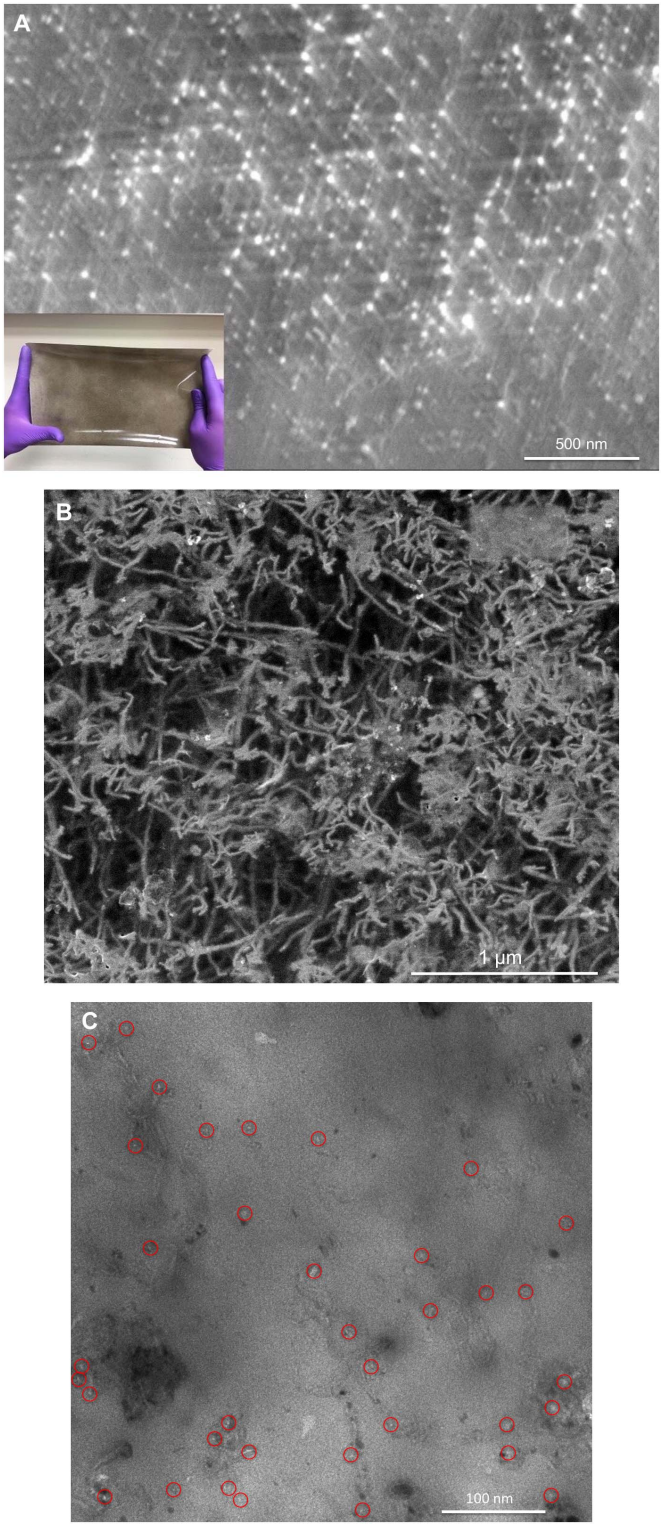

Fig. 1. Images of the membranes tested in this study. (**A**) SEM image of the CNT membrane surface, showing CNT tips emerging from the polymer. Inset shows the membrane sample without magnification. (**B**) SEM image of the surface of the CNT membrane using an imaging technique that uses high voltage without sputter coating to reveal the CNTs below the membrane surface. (**C**) TEM image of the CNT membrane in planar view, showing CNT pore openings, indicated by red circles, emerging from CNTs below the membrane surface.

diameter of the analyte, which is below the diameter of the largest CNTs. No defects are visible in SEM imaging, which has a resolution of approximately 1 nm, supporting the hypothesis that any defects present are most likely near or below this resolution limit. Similarly, no defects are visible in TEM imaging.

The rejection of dyes with a background ionic strength (IS) of 34 mM NaCl indicate that CNT entrance charge effects are important for both Malachite Green (MG) and FD&C Blue #1. The rejection of salts was substantially higher at the ISs tested than has been reported previously in salt rejection tests of CNT membranes, with rejections of >10% for NaCl (34 mM IS) and $MgSO_4$ (66 mM IS). In previous studies, no significant rejection of KCl was observed at IS higher than 10 mM through CNTs with IDs of 1.6 nm, although it is important to note that different testing conditions were used in these studies, including dead-end versus cross-flow modes and lower transmembrane pressures, both of which can result in lower observed rejections (*24*).

To assess CNT membranes' tolerance to being cleaned with oxidants, the salt rejection and permeability of CNT membranes were tested before and after immersion in 2000-ppm NaClO for 2 hours. The water permeability increased slightly, and salt rejection was not significantly changed after immersion. This result indicates that oxidant cleaning of these membranes is likely to be feasible, which would allow their use in fouling environments that would prove difficult for current polymeric NF, RO, or FO membranes, which are not tolerant toward oxidants, as well as potentially extending the useful life of CNT membranes in these environments (*2*, *25*).

Gas permeance testing was performed with a constant flux gas permeation system (fig. S2). The permeances increased slightly with pressure, as shown in Fig. 3A, which differs from the pressure-independent behavior predicted for Knudsen flow (*26*). The absence of a relationship between gas viscosity and selectivity is shown in Fig. 3B, indicating that viscous flow through large defects does not appear to explain this pressure dependence. The analyte/He selectivities of several gases, plotted against their molecular weights, are shown in Fig. 3C. The selectivities of the gases, particularly the hydrocarbon gases, deviated substantially from Knudsen selectivity, in which the individual gas selectivities would be correlated with the inverse square root of their molecular weights.

DISCUSSION

Knudsen selectivity has been observed in previous CNT membrane studies for CNTs with IDs larger than 1 nm, with the exception of hydrocarbons in sub–2-nm CNTs, which also did not follow this relationship, potentially due to the effects of surface diffusion (*4*). Previous studies of subnanometer CNTs aligned in zeolite membranes indicated significant deviation from Knudsen flow, including both non-Knudsen selectivity and non-Knudsen pressure-dependent permeance, for a wide range of gases studied, which was attributed to the increased role of surface diffusion transport in these small CNT pores (*26*).

In modeling studies of gas transport through pores at the nanoscale, the contribution of Knudsen flow to the overall pore flow is found to decrease as the ID of the pore decreases, with surface diffusion along the pore wall becoming the dominant transport mechanism below an ID of approximately 1.2 nm (*27*, *28*). The relative importance of surface diffusion continues to increase until the ID of the CNT approaches the diameter of the gases, at which point molecular sieving occurs, with gases rejected from the CNT entrance based on size (*28*). This modeling, along with the previous subnanometer CNT gas transport data, may offer an explanation for the deviation from Knudsen selectivity observed

Downloaded from http://advances.sciencemag.org/ on November 17, 2019

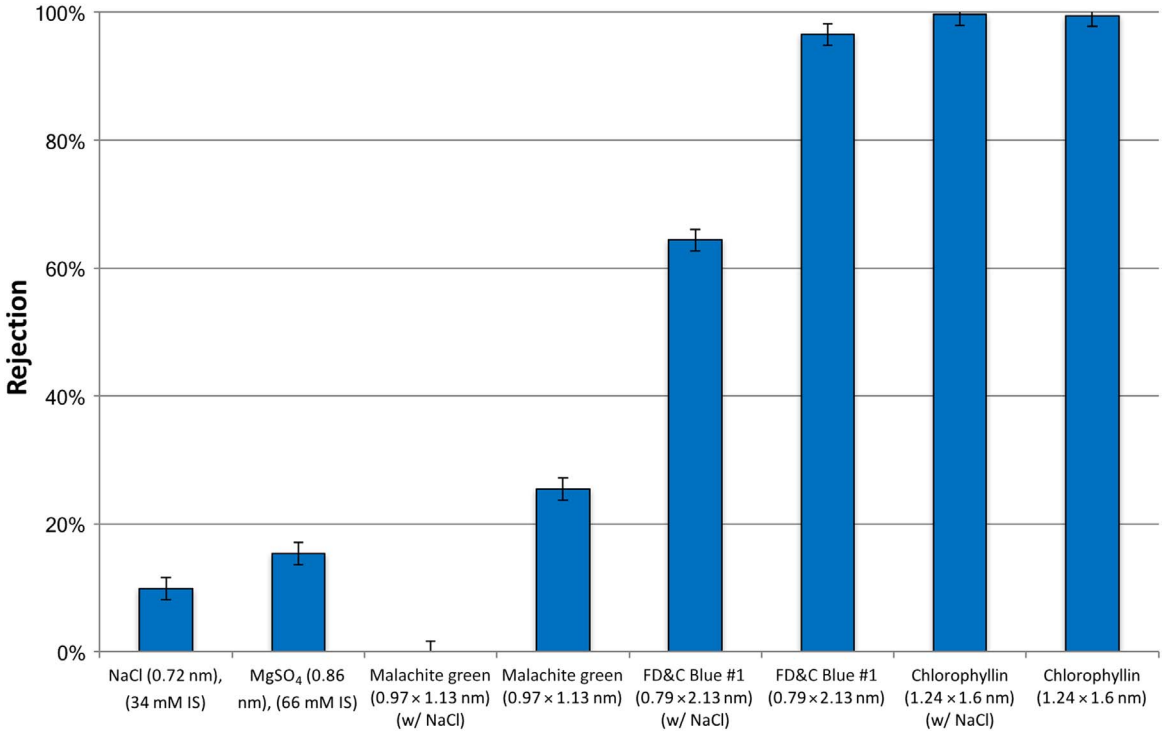

Fig. 2. Rejection of analytes in the aqueous separation tests, with molecular dimensions increasing from left to right. Rejection of dyes is shown with and without a background IS of 34 mM (NaCl) to examine the effects of Donnan exclusion versus steric exclusion on solute rejection.

in the CNT membranes of this study, as surface diffusion could be a significant contributor to gas transport.

CNT membranes with subnanometer pores for aqueous separations offer promising permeability, solute rejection, and chemical robustness characteristics. Oxidant-tolerant NF membranes that separate small dissolved solutes, but do not substantially desalinate or soften, may be particularly useful for water treatment, because they would not produce brine discharges or induce scale formation and could be routinely cleaned with bleach. The use of these membranes to remove pathogens and natural organic matter before the addition of residual disinfectant for distribution would prevent the formation of disinfectant by-products, which are currently difficult to prevent in drinking water systems (*29*, *30*). Desalination by RO or FO using CNT membranes of this type will require reduction in the size of the CNTs used, going from IDs of a maximum of 1.24 nm in this study to below 0.72 nm, the hydrated diameter of the sodium ion, to be practical. Gas separations using subnanometer CNT membranes based on size exclusion, preferential adsorption, and pore condensation effects are promising but will require further analysis using mixed gases across a range of pressures to identify optimal operating conditions for practical applications of these membranes.

MATERIALS AND METHODS

Aqueous separation tests

Determination of water, salt, and dye transport through the CNT membranes was performed using a standard RO test system, as shown in fig. S1. The membrane cells exposed 19.9 cm^2 of the membrane area to the feed solution, which was circulated through the membrane channels at 1.0 liter/min, resulting in a flow velocity of approximately 21 cm/s and a corresponding Reynolds number of approximately 1200. Temperature in the system was maintained at 20°C.

Water flux was determined gravimetrically, with the flux of any solutes across the membranes having a negligible impact on the final result. The determination of the hydraulic permeability coefficient was conducted at three pressures of 345, 690, and 1380 kPa, and the flux of water was found to be proportional to the feed pressure.

Solute rejection was determined via testing at 1400 kPa, and the concentration of the solutes was measured using an Oakton CON 11 conductivity meter with a "Consen91W" conductivity probe (for salts) and a Thermo Scientific GENESYS 10S UV-Vis spectrophotometer (for dyes). The feed concentration of both salts and dyes was found to be within the linear range of the instruments used; therefore, the rejection can simply be expressed as

$$\%R = \frac{S_f - S_p}{S_f} \quad (1)$$

where S_f is the signal in the feed (for example, optical absorbance and electrical conductivity) and S_p is the signal in the permeate.

After addition of a probe salt, the RO system was allowed to come to steady state over a period of 30 min before taking any measurements. The probe dyes used in this study, whose chemical structures are provided in fig. S3, were observed to adsorb to the membrane polymer matrix as well as the RO system tubing. To subtract this effect from the measurement of dye rejection, periodic samples of the solute rejection were taken until a stable value was obtained. Malachite green was observed to adsorb strongly over a period of several hours, with apparent rejection dropping from ca. 80 to ca. 20 to 40%. FD&C Blue #1 was observed to

Downloaded from http://advances.sciencemag.org/ on November 17, 2019

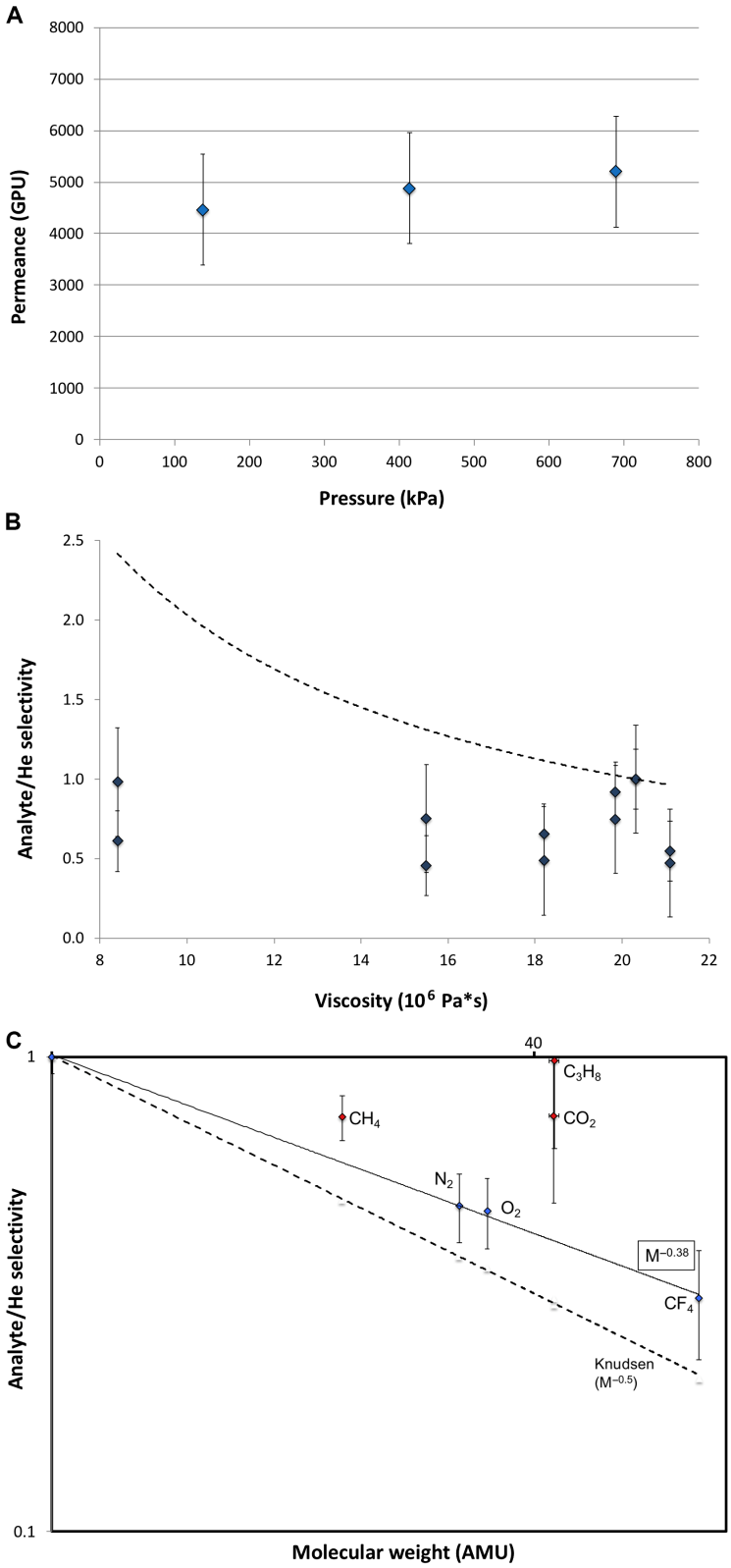

Fig. 3. Gas transport properties of CNT membranes. (**A**) Graph of the relationship between He permeance and pressure showing pressure dependence. GPU, gas permeation units. (**B**) Graph of the relationship between analyte/He selectivity and viscosity (viscous flow selectivity shown as a dashed line), indicating that no correlation with viscous flow is present. Viscosities for gases are taken from Yampolskii and Freeman (*27*). (**C**) Graph of the relationship between analyte molecular weight and analyte/He selectivity at 138 kPa. Knudsen selectivity is shown on the dashed line. Analyte selectivities deviate substantially from Knudsen, particularly the hydrocarbons and CO_2 (shown in red data points). AMU, atomic mass units.

Downloaded from http://advances.sciencemag.org/ on November 17, 2019

adsorb to a lesser degree, and no adsorption of chlorophyllin copper was observed.

The effect of charge screening of the dye molecules was investigated by measuring the rejection of the dye in the presence of 2000-ppm sodium chloride. Trials in which both salt and dye were present assumed that the contribution to the conductivity of the permeate sample was entirely due to the presence of the salt and that the optical absorbance of the permeate sample was entirely due to the presence of the dye. Because the addition of salt may change the adsorption of solutes in the membrane polymer matrix, periodic tests of rejection were conducted until the measured dye rejection was stable. Malachite green rejection in the presence of sodium chloride was always observed to be slightly negative, that is, the optical absorbance of the permeate solution was 2 to 6% higher than that of the feed solution, potentially indicating an extremely long (more than several days) desorption cycle. The rejection of sodium chloride in the presence of dyes was unchanged. During the experiments, membrane permeability fell by more than 50%, likely due to the accumulation of particulate material (for example, dust and rust particles) on the membrane surface; this was likely due to the absence of a particulate filter in-line in the RO system (*31*). After the initial permeability decline, it remained steady throughout testing, a phenomenon similar to initial permeability declines observed in conventional polymeric membrane testing (*1*).

Oxidation resistance and cleaning with sodium hypochlorite

To evaluate the membrane's ability to withstand cleaning via sodium hypochlorite ("bleach"), a 2000-ppm solution of sodium hypochlorite (Chlorox, ~8.25%) in deionized (DI) water was circulated through the RO test system in contact with previously tested AD membranes with no transmembrane pressure and at flow conditions identical to those used in RO testing. After 1 hour of exposure, the system was flushed thoroughly with DI water before the membranes were evaluated for sodium chloride rejection at a concentration of 2000 ppm. The bleach cleaning protocol increased membrane permeability slightly while not significantly changing the sodium chloride rejection, indicating that the CNT membrane rejection does not decrease upon exposure to bleach and that the recovered flux does not appear to be a result of degradation of the polymer matrix.

Gas permeance tests

The permeation of pure gases was determined using a constant pressure gas permeation system (*32*), as shown in fig. S2. Membrane samples were mounted with epoxy under brass discs, and the effective membrane area was determined with image analysis using ImageJ software.

Membrane samples were mounted in a permeation cell immersed in an air bath held at 35°C and were flushed on both sides with the feed gas for ~10 min before measuring permeance. The flux of gas was measured via a bubble flow meter at atmospheric pressure. Three pressures 138, 441, and 690 kPa of feed gas were tested across three representative membrane samples. Three series of gases were tested: (i) He, O_2, N_2, CH_4, CO_2; (ii) He, N_2, C_3H_8; (iii) He, N_2, CF_4. Membrane samples were not used for additional testing after being exposed to plasticizing or potentially plasticizing gases (CO_2, C_3H_8, CF_4).

SEM procedure

A unique imaging method for CNT in the polymer matrix was used. To visualize the CNT network embedded in the polymer, a high accelerating voltage (20 kV) was used to image an untreated sample (no sputter coating), which was well grounded through the use of silver paint. In the resulting image, the polymer was transparent, whereas the tubes were rendered opaque.

SUPPLEMENTARY MATERIALS

Supplementary material for this article is available at http://advances.sciencemag.org/cgi/content/full/4/3/e1700938/DC1

Supplementary Text

fig. S1. Experimental apparatus for RO testing.

fig. S2. Experimental apparatus for gas permeation testing.

fig. S3. Wireframe model of dye molecules.

table S1. Manufacturer specifications for CNTs.

table S2. Approximate enhancement factor for CNT composite membranes.

References (*33*–*40*)

REFERENCES AND NOTES

1. G. M. Geise, D. R. Paul, B. D. Freeman, Fundamental water and salt transport properties of polymeric materials. *Prog. Polym. Sci.* **39**, 1–42 (2014).
2. S. Surawanvijit, A. Rahardianto, Y. Cohen, An integrated approach for characterization of polyamide reverse osmosis membrane degradation due to exposure to free chlorine. *J. Membr. Sci.* **510**, 164–173 (2016).
3. B. J. Hinds, N. Chopra, T. Rantell, R. Andrews, V. Gavalas, L. G. Bachas, Aligned multiwalled carbon nanotube membranes. *Science* **303**, 62–65 (2004).
4. J. K. Holt, H. G. Park, Y. Wang, M. Stadermann, A. B. Artyukhin, C. P. Grigoropoulos, A. Noy, O. Bakajin, Fast mass transport through sub-2-nanometer carbon nanotubes. *Science* **312**, 1034–1037 (2006).
5. S. Joseph, N. R. Aluru, Why are carbon nanotubes fast transporters of water? *Nano Lett.* **8**, 452–458 (2008).
6. B. Corry, Designing carbon nanotube membranes for efficient water desalination. *J. Phys. Chem. B* **112**, 1427–1434 (2008).
7. X. Qin, Q. Yuan, Y. Zhao, S. Xie, Z. Liu, Measurement of the rate of water translocation through carbon nanotubes. *Nano Lett.* **11**, 2173–2177 (2011).
8. D. Cohen-Tanugi, J. C. Grossman, Water desalination across nanoporous graphene. *Nano Lett.* **12**, 3602–3608 (2012).
9. S. C. O'Hern, C. A. Stewart, M. S. H. Boutilier, J.-C. Idrobo, S. Bhaviripudi, S. K. Das, J. Kong, T. Laoui, M. Atieh, R. Karnik, Selective molecular transport through intrinsic defects in a single layer of CVD graphene. *ACS Nano* **6**, 10130–10138 (2012).
10. B. Mi, Graphene oxide membranes for ionic and molecular sieving. *Science* **343**, 740–742 (2014).
11. R. K. Joshi, P. Carbone, F. C. Wang, V. G. Kravets, Y. Su, I. V. Grigorieva, H. A. Wu, A. K. Geim, R. R. Nair, Precise and ultrafast molecular sieving through graphene oxide membranes. *Science* **343**, 752–754 (2014).
12. M. Kumar, M. Grzelakowski, J. Zilles, M. Clark, W. Meier, Highly permeable polymeric membranes based on the incorporation of the functional water channel protein Aquaporin Z. *Proc. Natl. Acad. Sci. U.S.A.* **104**, 20719–20724 (2007).
13. R. Das, M. E. Ali, S. B. A. Hamid, S. Ramakrishna, Z. Z. Chowdhury, Carbon nanotube membranes for water purification: A bright future in water desalination. *Desalination* **336**, 97–109 (2014).
14. B. S. Flavel, M. M. Kappes, R. Krupke, F. Hennrich, Separation of single-walled carbon nanotubes by 1-dodecanol-mediated size-exclusion chromatography. *ACS Nano* **7**, 3557–3564 (2013).
15. R. J. R. Uhlhorn, K. Keizer, A. J. Burggraaf, Gas transport and separation with ceramic membranes. Part I. Multilayer diffusion and capillary condensation. *J. Membr. Sci.* **66**, 259–269 (1992).
16. R. Andrews, *Separation of CO_2 from Flue Gases by Carbon-Multiwall Carbon Nanotube Membranes* (DOE Technical Progress Report, U.S. Department of Energy, 2001).
17. R. Singh, W. J. Koros, Carbon molecular sieve membrane performance tuning by *dual* temperature *secondary* oxygen doping (DTSOD). *J. Membr. Sci.* **427**, 472–478 (2013).
18. W.-W. Liu, S.-P. Chai, A. R. Mohamed, U. Hashim, Synthesis and characterization of graphene and carbon nanotubes: A review on the past and recent developments. *J. Ind. Eng. Chem.* **20**, 1171–1185 (2014).
19. N. Arora, N. N. Sharma, Arc discharge synthesis of carbon nanotubes: Comprehensive review. *Diamond Relat. Mater.* **50**, 135–150 (2014).
20. Z. Liu, Q. Zhang, L.-C. Qin, Determination and mapping of diameter and helicity for single-walled carbon nanotubes using nanobeam electron diffraction. *Phys. Rev. B* **71**, 245413 (2005).
21. R. McGinnis, Selective membranes formed by alignment of porous materials, PCT patent application PCT/US13/76559 (2013).

Downloaded from http://advances.sciencemag.org/ on November 17, 2019

22. T. Ratto, J. Holt, A. Szmodis, Membranes with embedded nanotubes for selective permeability, U.S. Patent 7,993,524 (2011).
23. S. Kim, J. R. Jinschek, H. Chen, D. S. Sholl, E. Marand, Scalable fabrication of carbon nanotube/polymer nanocomposite membranes for high flux gas transport. *Nano Lett.* **7**, 2806–2811 (2007).
24. F. Fornasiero, H. G. Park, J. K. Holt, M. Stadermann, C. P. Grigoropoulos, A. Noy, O. Bakajin, Ion exclusion by sub-2-nm carbon nanotube pores. *Proc. Natl. Acad. Sci. U.S.A.* **105**, 17250–17255 (2008).
25. R. Baker, *Membrane Technology and Applications* (Wiley, ed. 2, 2000).
26. A. Labropoulos, C. Veziri, M. Kapsi, G. Pilatos, V. Likodimos, M. Tsapatsis, N. K. Kanellopoulos, G. E. Romanos, G. N. Karanikolos, Carbon nanotube selective membranes with subnanometer, vertically aligned pores, and enhanced gas transport properties. *Chem. Mater.* **27**, 8198–8210 (2015).
27. Y. Yampolskii, B. Freeman, *Membrane Gas Separation* (Wiley, 2010).
28. A. W. Thornton, T. Hilder, A. J. Hill, J. M. Hill, Predicting gas diffusion regime within pores of different size, shape and composition. *J. Membr. Sci.* **336**, 101–108 (2009).
29. T. K. Nissinen, I. T. Miettinen, P. J. Martikainen, T. Vartiainen, Molecular size distribution of natural organic matter in raw and drinking waters. *Chemosphere* **45**, 865–873 (2001).
30. S. D. Richardson, *Disinfection by-Product: Formation and Occurrence in Drinking Water* (National Exposure Research Lab, U.S. Environmental Protection Agency, 2011).
31. E. M. Van Wagner, A. C. Sagle, M. M. Sharma, B. D. Freeman, Effect of crossflow testing conditions, including feed pH and continuous feed filtration, on commercial reverse osmosis membrane performance. *J. Membr. Sci.* **345**, 97–109 (2009).
32. S. M. Wiederhorn, R. J. Fields, S. Low, G.-W. Bahng, A. Wehrstedt, J. Hahn, Y. Tomota, T. Miyata, H. Lin, B. D. Freeman, S. Aihara, Y. Hagihara, T. Tagawa, Mechanical properties, in *Springer Handbook of Metrology and Testing*, H. Czichos, T. Saito, L. Smith, Eds. (Springer, 2011), pp. 339–452.
33. M. Majumder, N. Chopra, B. J. Hinds, Mass transport through carbon nanotube membranes in three different regimes: Ionic diffusion and gas and liquid flow. *ACS Nano* **5**, 3867–3877 (2011).
34. M. Mulder, Transport in membranes, in *Basic Principles of Membrane Technology* (Springer, ed. 2, 1996), pp. 224–227.
35. W. M. Haynes, *CRC Handbook of Chemistry and Physics* (CRC Press, ed. 91, 2010).
36. F. Fornasiero, J. B. In, S. Kim, H. G. Park, Y. Wang, C. P. Grigoropoulos, A. Noy, O. Bakajin, pH-tunable ion selectivity in carbon nanotube pores. *Langmuir* **26**, 14848–14853 (2010).
37. A. Akbari, P. Sheath, S. T. Martin, D. B. Shinde, M. Shaibani, P. C. Banerjee, R. Tkacz, D. Bhattacharyya, M. Majumder, Large-area graphene-based nanofiltration membranes by shear alignment of discotic nematic liquid crystals of graphene oxide. *Nat. Commun.* **7**, 10891 (2016).
38. Chlorine a6, http://chemspider.com/Chemical-Structure.4586363.html [accessed 8 August 2016].
39. Brilliant Blue FCF, http://chemspider.com/Chemical-Structure.18556.html [accessed 8 August 2016].
40. Malachite Green Chloride Salt, http://chemspider.com/Chemical-Structure.10820.html [accessed 8 August 2016].

Acknowledgments: We thank K. Kapalczynski, J. Curley, and A. R. Martinez for their assistance. **Funding:** This study was partially supported by the U.S. Department of Energy Office of Science, Office of Basic Energy Sciences under award number DE-FG02–02ER15362. This material is based on work supported by the NSF Graduate Research Fellowship Program under grant no. DGE-1610403. Any opinions, findings, and conclusions or recommendations expressed in this material are those of the authors and do not necessarily reflect the views of the NSF. We would also like to acknowledge the University of Connecticut (Department of Chemical and Biomolecular Engineering) and the GE Fellowship for Innovation. **Author contributions:** R.L.M. provided the membranes and assisted with developing test protocols. K.R., B.D.F., J.D.M., M.M.M., J.P., and K.A.S. performed gas transport measurements. J.R.M., J.R., and L.X. performed water transport measurements. K.R., X.S., M.A., and M.R.C. performed SEM imaging. X.S. and M.A. also performed TEM imaging. All authors contributed to writing and editing the manuscript. **Competing interests:** R.L.M. is the inventor on a patent application related to this work (PCT patent application PCT/US13/76559, 2013). J.R.M. is an advisor to Mattershift and owns <0.1% of the company's stock; K.R. is a part-time employee of Mattershift and owns <1% of the company's stock; R.L.M. is the founder and owner of Mattershift. The other authors declare that they have no competing interests. **Data and materials availability:** All data needed to evaluate the conclusions in the paper are present in the paper and/or the Supplementary Materials. Additional data related to this paper may be requested from the authors.

Submitted 21 March 2017
Accepted 2 February 2018
Published 9 March 2018
10.1126/sciadv.1700938

Citation: R. L. McGinnis, K. Reimund, J. Ren, L. Xia, M. R. Chowdhury, X. Sun, M. Abril, J. D. Moon, M. M. Merrick, J. Park, K. A. Stevens, J. R. McCutcheon, B. D. Freeman, Large-scale polymeric carbon nanotube membranes with sub–1.27-nm pores. *Sci. Adv.* **4**, e1700938 (2018).

Downloaded from http://advances.sciencemag.org/ on November 17, 2019

ScienceAdvances

Large-scale polymeric carbon nanotube membranes with sub–1.27-nm pores

Robert L. McGinnis, Kevin Reimund, Jian Ren, Lingling Xia, Maqsud R. Chowdhury, Xuanhao Sun, Maritza Abril, Joshua D. Moon, Melanie M. Merrick, Jaesung Park, Kevin A. Stevens, Jeffrey R. McCutcheon and Benny D. Freeman

Sci Adv **4** (3), e1700938.
DOI: 10.1126/sciadv.1700938

ARTICLE TOOLS http://advances.sciencemag.org/content/4/3/e1700938

SUPPLEMENTARY MATERIALS http://advances.sciencemag.org/content/suppl/2018/03/05/4.3.e1700938.DC1

REFERENCES This article cites 28 articles, 6 of which you can access for free
http://advances.sciencemag.org/content/4/3/e1700938#BIBL

PERMISSIONS http://www.sciencemag.org/help/reprints-and-permissions

Use of this article is subject to the Terms of Service

Science Advances (ISSN 2375-2548) is published by the American Association for the Advancement of Science, 1200 New York Avenue NW, Washington, DC 20005. The title *Science Advances* is a registered trademark of AAAS.

Copyright © 2018 The Authors, some rights reserved; exclusive licensee American Association for the Advancement of Science. No claim to original U.S. Government Works. Distributed under a Creative Commons Attribution NonCommercial License 4.0 (CC BY-NC).

Downloaded from http://advances.sciencemag.org/ on November 17, 2019